On the resilience assessment of complementary transportation networks under natural hazards

Chao Fang, Yanze Chu, Haoran Fu, Yiping Fang

Transportation Research Part D 109 (2022) 103331

Contents lists available at ScienceDirect

Transportation Research Part D

journal homepage: www.elsevier.com/locate/trd

On the resilience assessment of complementary transportation networks under natural hazards

Chao Fang [a], Yanze Chu [a], Haoran Fu [a,*], Yiping Fang [b]

[a] School of Management, Xi'an Jiaotong University, Xi'an, ShaanXi, 710049, China
[b] Laboratoire Génie Industriel, CentraleSupélec, Université Paris-Saclay, 3 Rue Joliot-Curie, 91192, Gif-sur-Yvette Cedex, France

ARTICLE INFO

Keywords:
Transportation networks
Resilience assessment
Natural hazard
Spatially Localized Failure
Monte Carlo simulation

ABSTRACT

Transportation systems are fragile when facing various natural hazards. To analyze the performance of these systems under disruption, this paper provides a holistic multi-phase model to assess the resilience of a transportation system consisting of multiple modes. The hazard scenarios for modeling strikes of typhoons are generated by the Spatially Localized Failure (SLF) model and Monte Carlo simulation. Then based on the simulation of typhoon scenarios, we assess the resilience of both single-mode systems and a complementary system of multiple modes. This method is applied to the high-speed rail network and civil aviation network in China under different typhoon intensity scenarios. Results show the different resilience characteristics of the two networks, and more importantly unveil the complementary effect between the two modes when suffering from damages. The improvement of system resilience due to the complementary effects provides a motivation for promoting cooperation between high-speed rail and civil aviation.

1. Introduction

Modern transportation systems play a cornerstone role in human mobility, economic development, and social stability. However, recent years have seen many disruptions of these systems, especially caused by natural hazards. For example, the Icelandic volcano eruption in 2010 caused more than 100,000 flights canceled (Stamos et al., 2015; Reichardt et al., 2018). More than 2000 miles of roadways and 500 miles of highways were affected in America under Hurricane Irene (Faturechi and Miller-Hooks, 2014). Typhoons landed in China 7.8 times on average per year, bringing severe disruptions to transportation systems such as roadblocks, train delays, and flight cancellations (Takagi et al., 2021). In view of the increasing frequency, destructive power, and extreme weather in the context of global climate change, it is imperative and valuable to study the impact of natural hazards on transportation systems. This calls for a quantifiable approach to assessing the resilience of transportation systems under natural hazards, in support of decision-makers for system protection and performance restoration.

Since Holling (1973) first proposed resilience in ecological systems and defined it as biodiversity, the term resilience has been broadly studied and applied to different disciplines. According to previous studies on resilience, the common recognition is its description of the systems' ability to sustain and bounce back under external disturbance (Wan et al., 2018; Fang and Zio, 2019). Regarding the resilience assessment of transportation systems, much work has been conducted on a single system. For example, Ip and Wang (2011) quantified the resilience of the rail system based upon the weighted sum of reliable passageways. Chen and Miller-Hooks (2012) provided an indication of network resilience for intermodal freight transport network that considers networks'

* Corresponding author.
E-mail address: haoranfu@xjtu.edu.cn (H. Fu).

https://doi.org/10.1016/j.trd.2022.103331

Available online 21 June 2022

topology as well as operational attributes. The metro system resilience was defined by D'Lima and Medda (2015) as the speed at which the number of passengers returns to normal. Janić (2015) developed a resilience assessment framework for air transport where resilience was considered as the ratio of remained flights under a large-scale disruptive event. Verschuur et al. (2020) analyzed resilience of ports using the number of affected days and the number of recovering days. Aghababaei et al. (2020) evaluated post-disaster performance of a large regional road network using the number of trips, traffic flows and travel time. Zeng et al. (2021) proposed a comprehensive framework for health management of a transportation system to increase system availability and resilience. Part of the literature assesses the resilience of a transportation system as the retained performance level during disruptions (Ip and Wang, 2011; Janić, 2015), while others focus on recovery characteristics like recovery speed (D'Lima and Medda, 2015), recovery capacity (Barker et al., 2013; Fang et al., 2016; Henry and Ramirez-Marquez, 2012), etc. But metrics in these researches cannot fully reflect the characteristics of system resilience, as resilience features are reflected on multi-phases, i.e. before, during, and after disruptions (Fang et al., 2019). Decision-makers may not be able to provide effective protection for transportation systems without a comprehensive understanding of system resilience.

Even if the resilience of one individual system has been well assessed, the interactions between multiple transportation systems may also affect the accuracy of assessment results due to the increased system complexity and interconnection. Passengers are usually distributed on geographical extensions with network structures, which are highly geographically interdependent (Zhang and Peeta, 2011). When one mode is disrupted, the others can provide alternative options to deliver delayed passengers under disruptive events. For urban transportation, there has been a stream of research considering disruption management for a transportation system consisting of metro networks and bus services. Jin et al. (2014) investigated bus network design to achieve a desired metro network resilience under potential disruptions. Many authors have considered bus bridging services as an operational response to a rail disruption (Wang et al., 2014; Jin et al., 2016; Liang et al., 2019; Luo and Xu, 2021). Van der Hurk et al. (2016) studied alternative shuttle services for closed public transport systems under budget constraints. Zhang and Lo (2018) studied the initiation time of substitute bus services for metro disruption management. As important components of the passenger transport systems, the high-speed rail and civil aviation systems have attracted more attention in terms of their competitive situation and cooperative prospects. For example, D'Alfonso et al. (2015) studied the impact of high-speed rail development on the civil aviation system in terms of the environment and social welfare. Given their impacts on consumer surplus and social welfare, Avenali et al. (2018) studied the strategic formation of the partnership of airline and high-speed rail systems. Zhou and Chen (2020) studied resilience of airports under severe weather events and the positive effects of high-speed rail as a substitution. Although these studies have expanded economic perspectives on the relationship between the high-speed rail and civil aviation systems, key questions on how their interconnection affects system performance under disruptive events remain unresolved. To our best knowledge, very few studies have studied related issues. Ouyang et al. (2015) studied the complementary effect between regular rail and airline systems on network accessibility. Baggag et al. (2018) considered a multi-modal transportation system of a city, and studied its coverage efficiency and robustness. Li and Rong (2019) studied the complementary effect of high-speed rail on the civil aviation network in terms of network connection efficiency. However, these studies measured system performance with static topological metrics, ignoring the dynamic performance of transportation systems when facing natural hazards.

To address the aforementioned issues, this paper proposes a holistic multi-phase resilience assessment model for complementary transportation systems under natural hazards. In particular, the approach integrates a group of resilience factors, including vulnerability, disruption rapidity, recovery rapidity, and recoverability. Resistance ability during disturbance and post-disaster recovery ability can be quantified by the proposed model simultaneously. Besides, the on-time departure rate of passengers is regarded as the time-dependent performance metric. In this study, the functional substitution effects between different modes at the same geographical location under disruptions are regarded as complementary. We analyze the resilience characteristics of the high-speed rail network (HRN) and civil aviation network (CAN), respectively, under typhoon disruption scenarios. It is found that the complementary effects improve the system resilience due to the different resilience characteristics of the two modes. Numerical results further show how their complementary relationship affects system resilience under different disruption scenarios. The effectiveness of enhancement strategies is quantified by scenario-based sensitivity analysis. Further, to validate the practical significance of the resilience assessment model and enhancement strategies, the proposed methods are applied to a real case of a typhoon event.

The remainder of the paper is organized as follows. Section 2 introduces a holistic multi-phase resilience assessment model. In Section 3, HRN and CAN are introduced, and hazard scenarios for typhoons are generated. Section 4 presents the evaluation results by applying the proposed framework to the HRN and CAN under typhoon scenarios with different intensities. Further, Section 5 discusses the application of resilience enhancement strategies to a specific typhoon and Section 6 provides conclusions.

2. The resilience assessment metrics

A brief summary of the analysis framework in this paper is illustrated by Fig. 1. It consist of three modules, including transportation system, hazard scenario generation and resilience assessment. In this section, we first introduce the resilience assessment metrics.

Being consistent with most literature (Chen and Miller-Hooks, 2012; Henry and Ramirez-Marquez, 2012; Fang et al., 2019, etc.), we define the resilience of a transportation system as its inherent capacity to resist disaster and recovery from disruptions with a reasonable time frame. It can be reflected in the fluctuation of the system performance curve within a disrupting time horizon. In this paper, we use the time-dependent system performance function curve to better describe resilience and its related attributes in different phases, as Fig. 2 shows. The vertical axis, $P(t)$, represents the performance level over time and the horizontal axis denotes

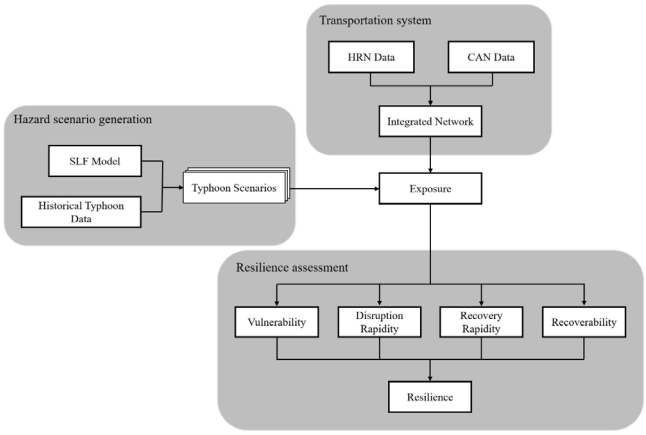

Fig. 1. Flow chart of the resilience analysis process.

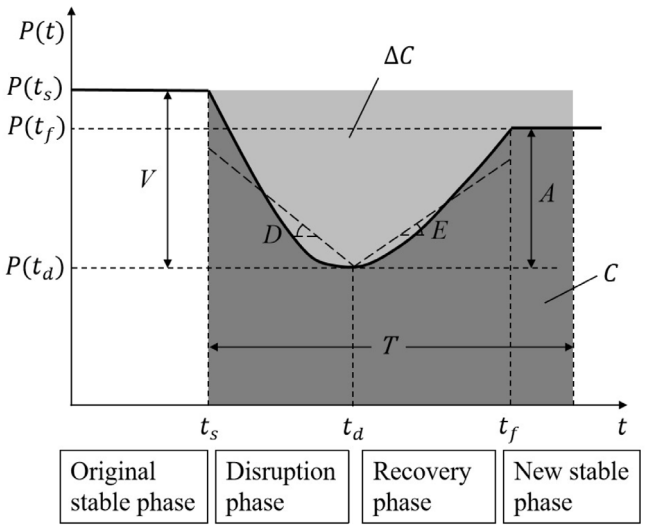

Fig. 2. Graphical description of system resilience.

time. As described in Fig. 2, the system goes through four phases, including the original stable phase, disruption phase, recovery phase, and new stable phase.

In the original stable phase, the system operates as normal, where the original system performance is denoted as $P(t_s)$. The disruptive events appear at time t_s, and the system performance curve reduces until it reaches the worst level $P(t_d)$ at time t_d. The time point marks when the system reaches its worst performance, but does not necessarily mean that recovery operations only occur after that time. Although it may be difficult to determine this exact time point during continuous disruptions, there are many representative events (e.g., lifting the ban on the scheduling of trains/flights) and collectable data (e.g., the number of served passengers on the valley floor) that are helpful in analyses. These are practical methods to determine the time point. Then the system performance begins to recover from the worst level until it returns to a new equilibrium level $P(t_f)$. In reality, $P(t_f)$ could be the same as, close to, or better than the initial performance according to the actual requirements and available resources (Wan et al., 2018).

Most of the studies on transportation resilience quantify a static resilience value only, neglecting the properties that the resilience of a complex system consists of Adjetey-Bahun et al. (2016). To explore the complementary resilience of multiple transportation systems, differences in resilience of the systems in each phase of disruption need to be addressed. These differences reveal the resilience characteristics of systems in different phases, which give a clue to the potential of cooperation between systems to improve the complementary resilience. Specifically, we define four metrics to characterize different aspects of resilience, including vulnerability (V), disruption rapidity (D), recovery rapidity (E), and recoverability (A), as shown in Fig. 2. The former two metrics can represent the resistance capability of a network while the latter two can reflect the recovery capability of a network.

Vulnerability (V) describes a system's susceptibility to disruptions that may decrease network serviceability (Berdica, 2002). It is one of the representative indicators in the disruption phase, which is measured as follows,

$$V \equiv P(t_d) - P(t_s). \tag{2.1}$$

Recoverability (A) is a resilience indicator for the new-stable phase, which is usually used to describe the system's ability to return to a new stable level promptly (Baroud et al., 2014). The recoverability metric can be quantified as the total performance recovery to performance loss as follows,

$$A \equiv P(t_f) - P(t_d). \tag{2.2}$$

Disruption rapidity (D) is able to identify the system's absorption capability under disruptions. The metric can be approximated by the average slope of the performance curve in the disruption phase (Nan and Sansavini, 2017). Recovery rapidity (E) is one of the representative characteristics in the recovery phase and focuses on the recovery speed (Adams et al., 2012). It can then be calculated by the average slope of the performance curves in the recovery phase. These two metrics can be expressed by

$$D \equiv \frac{\int_{t_s}^{t_d} [P(t) - P(t_s)]\mathrm{d}t}{t_d - t_s}, \tag{2.3}$$

$$E \equiv \frac{\int_{t_d}^{t_f} [P(t) - P(t_d)]\mathrm{d}t}{t_f - t_d}. \tag{2.4}$$

To compare performance characteristics of one system under different disruptions or different systems under one disruption approximately, a unified length of time interval T is necessary. This setting guarantees that all cases have the same baseline in time period that is under concern. Then the system resilience is defined as

$$R \equiv \frac{\int_{t_s}^{t_s+T} P(t)\mathrm{d}t}{P(t_s) \cdot T}. \tag{2.5}$$

Using the four metrics defined above, it is reformulated as

$$R = \frac{P(t_s) \cdot T + V \cdot T + D \cdot (t_d - t_s) + E \cdot (t_f - t_d) + A \cdot (T + t_s - t_f)}{P(t_s) \cdot T} \tag{2.6}$$

$$= 1 + \frac{V \cdot T + D \cdot (t_d - t_s) + E \cdot (t_f - t_d) + A \cdot (T + t_s - t_f)}{P(t_s) \cdot T}. \tag{2.7}$$

The system resilience defined here is actually the ratio between the cumulative performance under failure and the cumulative performance under baseline settings. The denominator in (2.6) is the cumulative performance without disruption while the numerator is the denominator minus performance loss during the disruption. Consistent to definitions, system performance is decreasing with V and D, but is increasing with E and A. Using the shadow areas illustrated in Fig. 2, the system resilience is also expressed by

$$R = \frac{C}{C + \Delta C}, \tag{2.8}$$

where C and ΔC are the areas of shaded regions illustrated in Fig. 2. This metric R reflects the surviving ratio of a system's performance during a disaster.

3. Modeling transportation networks under natural hazards

This section provides the problem settings in this paper. We consider a high-speed rail network (HRN) and a civil aviation network (CAN). Specifically, we apply these networks in China, which suffer from various natural hazards (Chen and Wang, 2019). Then, we use a spatially localized failure model to simulate hazard scenarios under which the resilience performance of the networks are analyzed.

3.1. Transportation network settings

In our model, the HRN is described by a graph $G^0 = (\mathcal{N}^0, \mathcal{L}^0, \Gamma^0)$, where $\mathcal{N}^0$ denotes the node set for stations, $\mathcal{L}^0$ denotes the link set for railways and Γ^0 denotes all trains of HRN in service. The daily travel demand of all trains are given as $Q^0 \equiv \{Q^0_\gamma | \gamma \in \Gamma^0\}$. There are a large number of small yards that are not included in the graph, while they have been absorbed along railway links. Hong et al. (2015) and Fang et al. (2020). Multiple high-speed rail stations in the same city are merged, for example, we merge Beijing South rail Station and Beijing North rail Station into one. This simplification helps us exclude the impact of the inconvenience (or disutility) of local infrastructures, since this paper focuses on the system performance of networks rather than passengers' behaviors. The transfer behavior of passengers is deterministic where a passenger will choose the alternative if there is available capacity (in a increasing order of cost if there are multiple alternatives) and will forgo travel otherwise. According to the high-speed rail layout and the official website of China rail Customer Service Center, the data of 212 stations and 238 links operating in 2018 are collected. Based on the layout, 7157 high-speed rail trips in the timetable of a normal weekday are selected, including 3262 G-prefix trains

(a) The high-speed rail network (b) The civil aviation network

Fig. 3. HRN and CAN in China.

(bullet trains with maximum speed reaches to 350 km/h), 2697 D-prefix trains (electric multiple unit trains with maximum speed reaches to 250 km/h), and 1198 C-prefix trains (intercity rail service with maximum speed reaches to 350 km/h). The illustration of Chinese HRN is shown in Fig. 3(a).

Similarly, the CAN is represented by $G^1 = (\mathcal{N}^1, \mathcal{L}^1, \Gamma^1)$, where $\mathcal{N}^1$ is the node set for airports, $\mathcal{L}^1$ is the link set for flights between two airports, Γ^1 denotes all flights. The daily travel demand of all flights are given as $Q^1 \equiv \{Q^1_\gamma | \gamma \in \Gamma^1\}$. Multiple airports in the same city are also merged. For example, Shanghai Hongqiao International Airport (with SHA as its IATA code) and Shanghai Pudong International Airport (with PVG as its IATA code) are combined into Shanghai Airport. According to CAAC (Civil Aviation Administration of China) and VariFlight® Map, the data of 222 airports and 2565 domestic flights are collected. The illustration of Chinese CAN is shown in Fig. 3(b).

We apply a day-to-day setting of traffic flows, which means the system performance is measured in the daily number of passengers.[1] This setting considers aggregate demands that have been served by trains/flights to estimate the system performance. For each network, the performance in the original stable phase is then defined:

$$P^m(t_s) = \sum_{\gamma \in \Gamma^m} Q^m_\gamma, \tag{3.1}$$

where Q^m_γ is the travel demand of transport mode m (0 for HRN and 1 for CAN) on train/flight γ. To determine the performance of a damaged network, we define the set of failed trains/flights as $\Gamma^{m,f}$ for mode m. Then, if the two modes are independently considered, the system performance of mode m at $t = t_d$ is measured by

$$P^m(t_d) = P^m(t_s) - \sum_{\gamma \in \Gamma^{m,f}} Q^m_\gamma. \tag{3.2}$$

3.2. Hazard scenario generation

Natural hazards (i.e. typhoons, floods, landslides, etc.) are among the main causes of large-scale disruptions of transportation systems. Due to high uncertainty and suddenness, natural hazards are generally difficult to estimate and predict. In this paper, we use a spatially localized failure (SLF) model to describe typhoon scenarios. The SLF model is useful to model disasters with random origins and determined ranges (Ouyang et al., 2019). The uncertainty of affected areas in typhoon scenarios is based on the data of typhoons passing through China from 2001 to 2021. Natural hazards like typhoons can cause disruptions of multiple links/nodes in a localized area. In the SLF model, all components of a system within a localized area of a natural hazard suffer from the impact while components outside are not affected (Fang et al., 2019). Since natural hazards often occur in a limited range, the disruption is local from the perspective of the global network.

To model SLFs, the first thing is to define a spatially localized impact area. Three common patterns are illustrated in Fig. 4, including node-centered, circle-shaped and district-based failure areas (Ouyang et al., 2019). Considering the large scope of the nationwide transportation networks and the province-based operations in practice, we apply the district-based pattern hereafter. Each province is regarded as a district in our model. A hazard scenario can be denoted by $\boldsymbol{S} = [s_1, s_2, \ldots, s_K]$ where s_k denotes the state of district k: $s_k = 1$ if the natural disaster attacks district k, being 0 otherwise. The failure state of all components are represented by $\boldsymbol{X} = [x_1, x_2, \ldots, x_I]$ and let $\boldsymbol{X}_k$ be that of all components in district k. Components refer to links and nodes of HRN and CAN. By a failure of a component, we mean that a train/flight or a station/airport is not functional.

[1] As the consequence, we do not consider within-day timetable or scheduling of trains/flights in our model. This simplification is further discussed in Section 6.

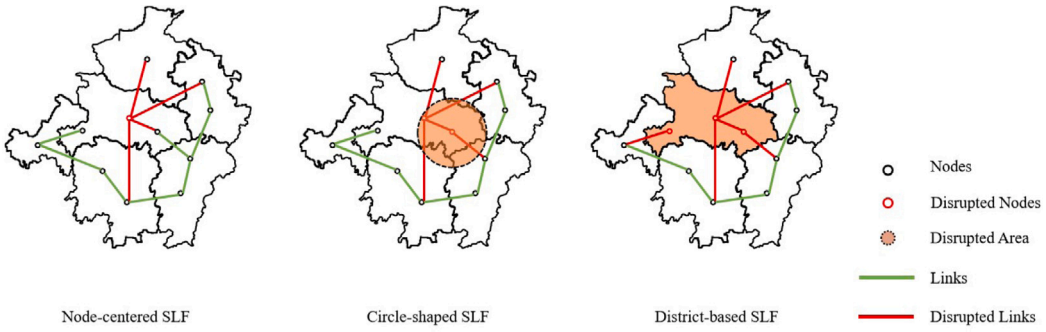

Fig. 4. SLF models.

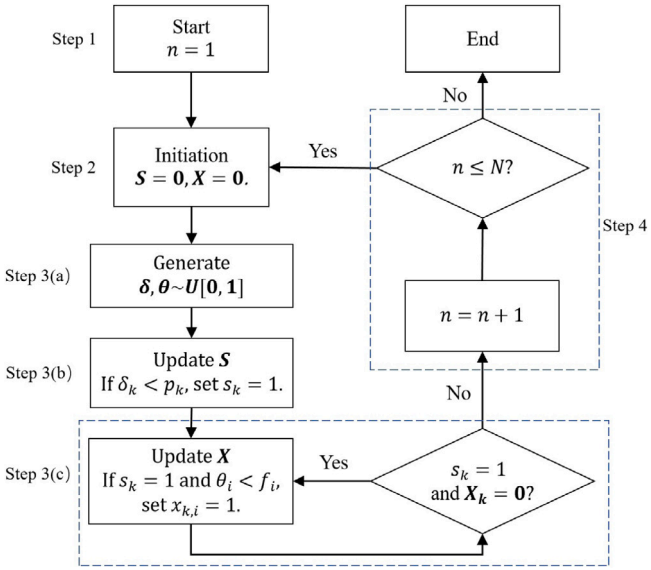

Fig. 5. Flow chart for generating hazard scenarios.

To generate a random hazard scenario, the Monte Carlo method and a probabilistic model are used. The specific process of generating hazard scenarios is illustrated in Fig. 5. In Step 1, define the total number of iterations N and set the iteration number n to equal 1. In Step 2, initiate the state vector of districts $\boldsymbol{S} = \boldsymbol{0}$ and the state vector of components $\boldsymbol{X} = \boldsymbol{0}$. In Step 3, firstly, generate a uniformly distributed random number $\delta_k \sim U(0,1)$ for each district k and another $\theta_i \sim U(0,1)$ for each component i. Secondly, compare δ_k with disaster occurrence probability p_k of district k given by data in history. If $\delta_k < p_k$, the district k is affected by the disaster and thus $s_k = 1$; otherwise, $s_k = 0$. Thirdly, if a district is attacked by a natural disaster (i.e., $s_k = 1$), then the failure probability f_i of component i is compared with the uniformly distributed random number θ_i. If $\theta_i < f_i$ (i.e., component i is out of service), then set $x_{k,i} = 1$. If a district is set to be affected and all components in that district hold undamaged, then the states of components in that district are reassigned. In Step 4, the iteration number is judged to decide whether the algorithm ends.

4. Resilience analysis of HRN and CAN under typhoons

In this section, we will analyze the performances of Chinese HRN and CAN, respectively, under typhoon scenarios. As brief conclusions, we find that resilience metrics of the two networks show that they have apparent differences in resilience characteristics. To demonstrate the complementary effect between the two networks due to the different characteristics in resilience, we compare a parallel system of the two networks with a complementary system. In the parallel system, HRN and CAN are operated separately and the system performance is a straightforward summation of the two networks. While in the complementary system, HRN and CAN cooperate as a supernetwork in which convenient transfers are provided to travelers. Further, sensitivity analyses are conducted to verify the complementary effect between the two networks in different parameter settings and to explore resilience enhancement policies.

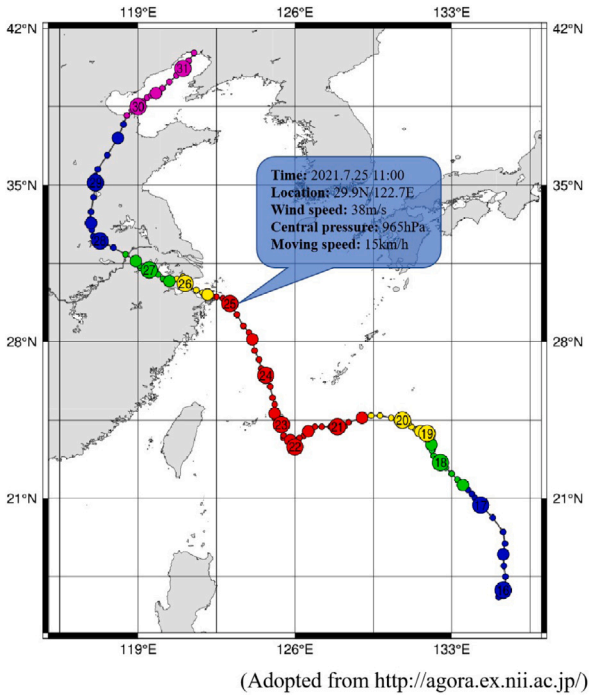

Fig. 6. A sample from the dataset of typhoons.

Table 1
Grades and impacts of typhoons.

Grade	Wind speed (m/s)	Impact on networks in localized areas	
		CAN	HRN
T1	17.2–24.4	Minor disruption	No significant impact
T2	24.5–32.6	Major disruption	Minor–Major
T3	≥32.7	Complete disruption	Major-Complete

4.1. Typhoon scenarios and component failures

According to the official website 'Weather China', 104 typical typhoons landed in China from 2001 to 2021, and thus data of all these typhoons are collected. Fig. 6 shows a sample from this dataset. By analyzing this representative historical dataset, the typhoon classification and the corresponding impacts are shown in Table 1. In this work, typhoons are classified into three categories, i.e., T1, T2, and T3. The corresponding impacts of different typhoons refer to the Railway Technical Management Regulations (page 104) and Civil Aviation Industry Standards of China (MH/T 3011.18-2006). Note that the impacts described here are approximated implementation references in policies, which will be characterized by specific parameters later in our model. In the T1-grade typhoon scenario, no facilities are damaged and HRN can provide train services normally. However, the operation of flights depends on the real situation: small and medium-sized passenger aircraft in downwind conditions cannot take off normally, which is referred to as minor disruption in the table. In the T2-grade typhoon scenario, speed limits are imposed on some trains in windy areas. For CAN, the majority of flights are prohibited from providing transport service. In the T3-grade typhoon scenario, the majority of trains and all flights in typhoon-affected regions would be delayed.

The occurrence probability and wind speed of typhoons are given by the historical data at the province level. We use the maximum speed of a typhoon observed in a province as the wind speed. For different damage strengths of typhoons (i.e., wind speeds in our model), components of transportation networks shall have different failure probabilities. Failure probability of independent components in a system is commonly described by fragility curves (e.g., Panteli and Mancarella, 2015; Argyroudis et al., 2020), which usually has a lognormal form,

$$f(x) = \phi[\frac{1}{\beta}\ln(\frac{x}{k})] \tag{4.1}$$

where $\phi(x)$ is the cumulative distribution function of normal distribution. Due to the lack of detailed information at the component level, we assume that independent components are equally maintained and thus have the same fragility curve. Considering standards in regulation references, we set parameters $\beta = 0.2, k = 20$ for CAN and $\beta = 0.2, k = 30$ for HRN. These two functions specify the

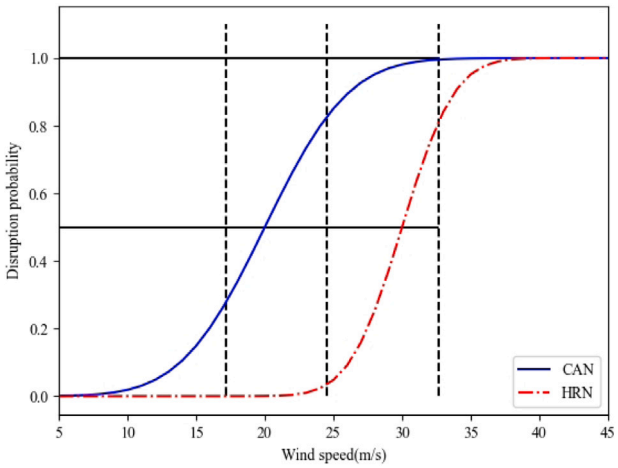

Fig. 7. Fragility curves of components under typhoons.

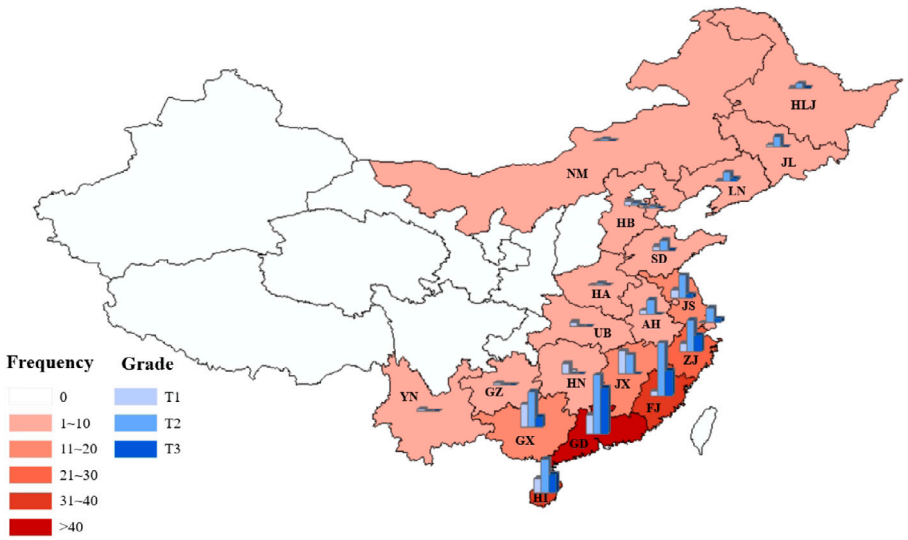

Fig. 8. Historical data of typhoons in provinces of China from 2001 to 2021.

failure probability f_i of component i in the two networks for given wind speeds of a typhoon. We then apply these fragility curves illustrated by Fig. 7 for HRN and CAN components in this study.

According to the classification in Table 1, Fig. 8 shows the geographical distribution of typhoon hazards. Intuitively, southeast coastal areas are typhoon-prone. The affected range varies with typhoon grades, as shown in the histogram. The T1-grade typhoon has a smaller scope of effect and 8 provinces have been affected, among which Guangdong (GD), Fujian (FJ), and Hainan (HI) are the top 3 provinces. It is shown that 11 provinces in China have been exposed to T2-grade typhoons and Guangdong (GD), Hainan (HI), Fujian (FJ), Guangxi (GX), Zhejiang (ZJ) have relatively high frequencies. The T3-grade typhoon is destructive and widespread that transportation facilities in 18 provinces need to take typhoon countermeasures, especially Guangdong (GD), Fujian (FJ), and Zhejiang (ZJ). The higher grade of typhoon hazards leads to a larger affected area. Based on the information above, typhoon disruption scenarios can be generated.

To apply the resilience assessment model, some other parameters in our model need to be specified. (1) We suppose that no trains or flights are disrupted or enhanced permanently, meaning the recoverability equals 1, or $A = -V$. (2) The resilience curve in the disruption phase is assumed to be linear, and the length of the disruption phase is approximated by the duration time of a typhoon. Considering the duration time of typhoons in the dataset (varies from 1 h to 70 h), we set $T = 72$ h. (3) To simplify the

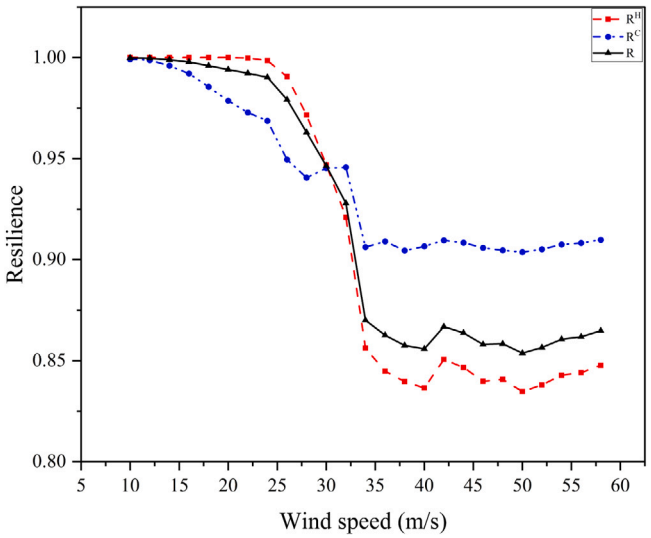

Fig. 9. Resilience of HRN and CAN under typhoon scenarios.

Table 2
Resilience factors for networks in typical typhoon scenarios.

Typhoon grade	Network	Resilience factors ($\times 10^4$)			
		V	D	E	A
T1	HRN	−1.31	−0.05	0.99	1.31
	CAN	−35.0	−1.27	17.5	35.0
T2	HRN	−93.4	−3.27	3.89	93.4
	CAN	−76.4	−2.67	25.5	76.4
T3	HRN	−274	−8.00	8.55	274
	CAN	−108	−3.15	26.9	108

base model, we consider fixed backup capacity ratio and fixed recovery rate for each network. But CAN is assumed to have a fairly higher recovery rapidity (i.e. shorter required recovery time) than HRN, which is consistent with reality.[2]

4.2. Resilience of independent HRN and CAN

According to the resilience assessment metrics in Section 2, the resilience values under typhoon scenarios with different damage strengths are calculated, which are illustrated in Fig. 9. In line with intuition, with the increase of the typhoon magnitudes, the resilience values of both HRN and CAN, R^H and R^C respectively, are decreasing, and so is the resilience R of the system involving both networks. That is because the high magnitude of typhoons causes more severe damages and thus more loss of system performance. However, the decreasing trends of the two networks vary with different scenarios. (1) In T1-grade typhoon scenarios, the resilience of HRN keeps almost unchanged, but that of CAN decreases a lot. This implies that HRN has a greater resistance capacity than CAN. (2) In T2-grade typhoon scenarios, both networks suffer great decreases in resilience. (3) In T3-grade typhoon scenarios, both networks are vulnerable and thus keep low resilience levels, but CAN is slightly better due to its promising nature in recovery rapidity.

Resilience assessment of HRN and CAN show their different characteristics under different typhoon magnitudes. Table 2 gives the value of resilience factors for the two systems to reflect the different resilience characteristics. In T1-grade typhoons, CAN has much larger values of vulnerability and recovery rapidity than HRN, which means CAN is more fragile but recovers faster. In T2-grade typhoons, CAN still shows a great recovery rapidity, but both networks suffer significant damages. In T3-grade typhoons, CAN retains high recovery rapidity, and HRN suffers a greater vulnerability. These metrics imply a clear path to enhance the complementary resilience of the whole transportation system: strengthening the alternative role of HRN in weak typhoons due to its resistance ability, and strengthening the alternative role of CAN in strong typhoons due to its recovery rapidity. These findings imply that cooperation between the two networks should have a good potential to improve the complementary resilience of the whole transportation system. In the next section, we will examine this idea.

[2] To extend our results with respect to this setting, we will provide sensitivity analysis of recovery time later in Section 4.4.

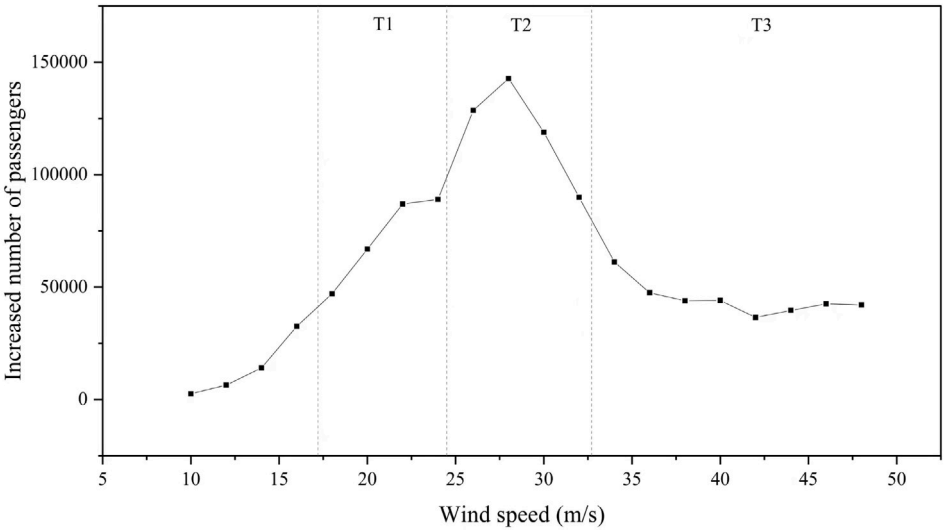

Fig. 10. Increased number of passengers due to complementary effects.

4.3. System resilience considering complementary effects

In this section, we investigate an integrated supernetwork of the two modes considering complementary effects. Specifically, the complementary effects mean that the two modes are well connected (e.g., by transportation hub of the two modes, or shuttle bus between stations) at cities with stations of both modes so that travelers treat the two modes as equal alternatives. In another word, the transfer cost between the two modes are set to be very small compared to the travel cost. For the convenience of expressions, we call this network a complementary system of the two networks and denote its resilience value as R'.

As a benchmark for comparison, we also consider a combined network of the two modes without complementary effects. In this network, the transfer cost between the two modes at one city is so high that travelers always choose other paths in the same mode or cancel their trips. This means that the substitution of alternative paths only exists in each individual network. In contrast to the complementary network, we call this network an integrated network and denote its resilience value as R.

The increased number of passengers of the complementary system compared to the combined system in typhoon scenarios is depicted in Fig. 10. Comparisons of results in these two systems show that the complementary effects between HRN and CAN improve system resilience, which results in a great number of increased passengers that reaches a peak of nearly 150,000 per day. This improvement excludes the summation effect of resilience values of the two separate networks. The improvement is due to the different characteristics of the resilience of the two networks. To explain this, notice that the number of passengers increases significantly with wind speed in T1-grade typhoon scenarios. This is because when facing weak typhoons, HRN has strong resistance capability and it plays the key role in the resilience of the complementary system. In T2-grade typhoon scenarios, this advantage due to the complementary effects increases first and then decreases quite a lot because both networks suffer great loss in performance and thus the complementary effect is weakened. For T3-grade strong typhoons, the advantage does not follow the decreasing trend to vanish, which is due to the strong recovery capability of CAN that supports the complementary effect in these scenarios.

Our results verify the positive role of complementary effects between the two networks. This implies that cooperation between HRN and CAN is necessary under hazard scenarios. In recent years, transport authorities have actually recognized the need for cooperation between these two systems and have implemented some cooperative measures. For example, Shanghai Rail Administration and China Eastern Airlines Corporation Limited signed a cooperation agreement on air–rail combined transportation products where passenger tickets and high-speed rail tickets related to Shanghai Hongqiao Station can be bought together on the sales platform of China Eastern Airlines; Recently, the agreement named "Promoting Strategic Cooperation Agreement on Air–Rail Intermodal Transport" has been signed between CAAC and China rail Corporation to promote the development of air–rail combined transport and establish integrated hub transportation stations. Further cooperation between high-speed rail and aviation systems is needed in the future, such as building more transportation-hub nodes, reducing transfer costs, and offering special discounts for intermodal fares. To further examine the complementary effect in more settings, we will provide sensitivity analysis in the next section.

4.4. Sensitivity analysis for enhancement strategy

In this section, we will discuss the impacts of two factors that are approximated in the resilience assessment model: the spare capacity and the recovery rapidity. The influences of these two factors on system resilience in different typhoon scenarios are shown by Fig. 11. Dashed curves in red depict the resilience of the complementary system corresponding to change of spare capacity or

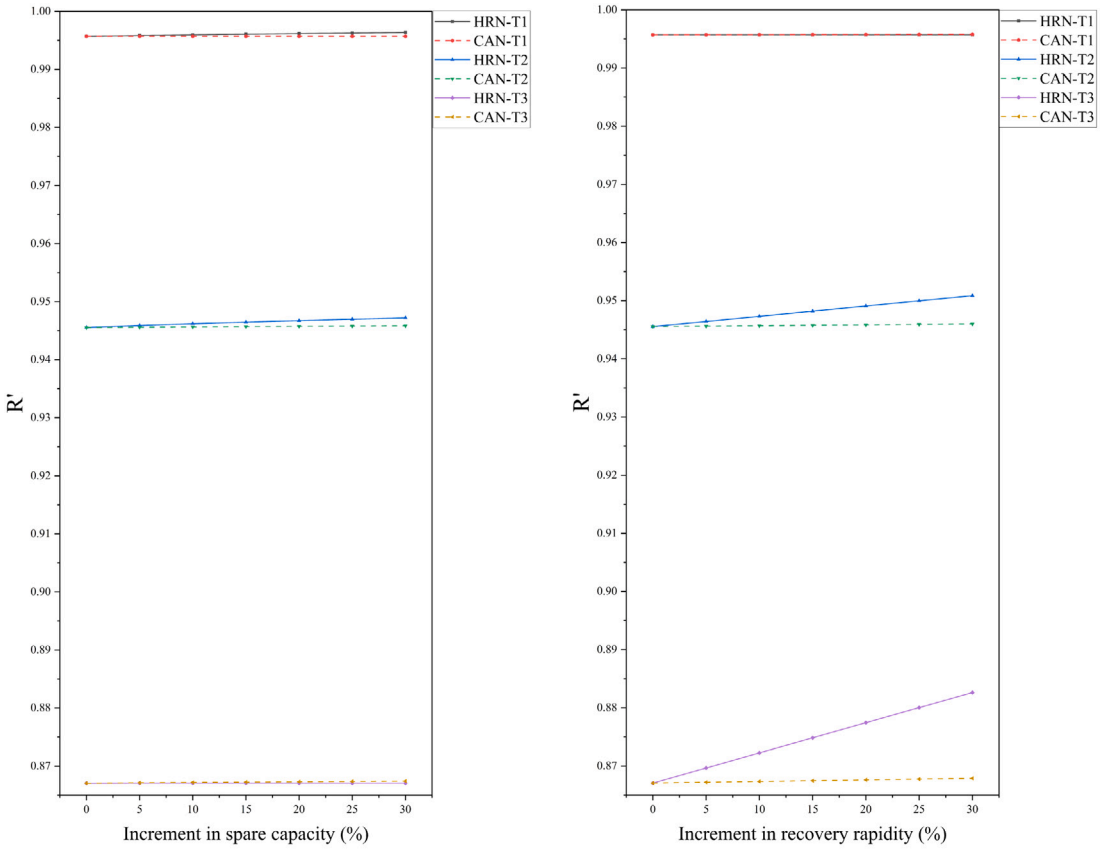

(a) Spare capacity in T1-grade typhoon scenarios (b) Recovery rapidity in T1-grade typhoon scenarios

Fig. 11. Sensitivity analysis of spare capacity and recovery rapidity. (For interpretation of the references to color in this figure legend, the reader is referred to the web version of this article.)

recovery rapidity in HRN, while solid curves in blue depict the resilience of the complementary system corresponding to change in CAN. The results vary a lot in different typhoon scenarios. (1) In T1-grade typhoon scenarios, increasing the spare capacity of HRN is more effective to enhance system resilience. This is due to the fact that HRN is almost undamaged in T1 typhoon scenarios, thus its spare capacity helps to serve passengers of disrupted flights in CAN. (2) In T2-grade typhoon scenarios, increasing the spare capacity of HRN is more effective. (3) In T3-grade typhoon scenarios, increasing recovery rapidity of HRN significantly enhances system resilience. This is because, in strong typhoons, both HRN and CAN are badly affected (either disrupted or damaged), and thus the spare capacity of either mode does not help much. As HRN has a much larger transport capacity, increasing the recovery rapidity (or decreasing the necessary time for repairing) of HRN deserves much more effort than that of CAN. This suggests that when facing strong typhoons, reducing the recovery time of HRN (by means such as infrastructure enhancement, pre-arranged rescue personnel and equipment) is more effective in the improvement of system performance. In summary, both the spare capacity and recovery time affect system resilience considerably but vary much in different typhoon scenarios.

It is noticed that enhancement of CAN has comparatively little influence on system resilience in Fig. 11. Considering that HRN has a much larger transport capacity than CAN in China (approximately 8:3), it is fair to argue that these implications may not be appropriate for other settings. Therefore, it is necessary to study the influence of different transport capacity ratios between the two networks. To exclude the effect of change in demand, we fix the total demand and vary the ratio between the transport capacity of HRN and CAN. Fig. 12 shows that increasing transport capacity of CAN has, respectively, a negative effect of system resilience in T1-grade typhoons, almost no effect in T2-grade typhoons, and a positive effect in T3-grade typhoons. This is consistent with the resilience characteristics of CAN, i.e. high vulnerability and high recovery rapidity. This result suggests that to benefit system resilience, we should increase the transport capacity of CAN in typhoon-prone provinces and increase the transport capacity of HRN in provinces suffering mostly weak typhoons.

5. Case study on Typhoon Mangkhut

Super Typhoon Mangkhut is one of the representative typhoon events affecting Chinese transportation systems in recent years because of its huge and lasting destructive power. It landed in Guangdong (GD) province on September 16, 2018 with the maximum

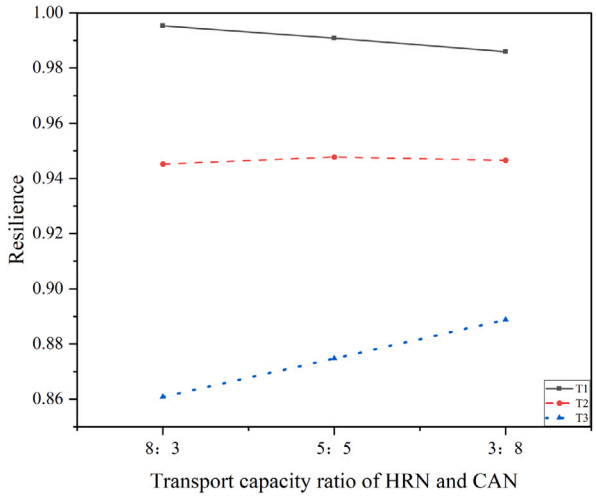

Fig. 12. System resilience considering transport capacity ratio.

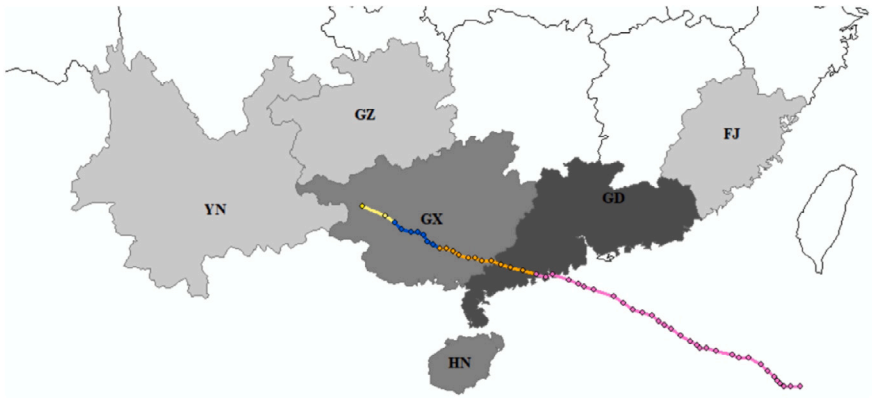

Fig. 13. The path and affected provinces of Typhoon Mangkhut.

wind speed reaching 50 m/s, causing more than 1500 trains delayed and 1800 flights canceled. After landing, the typhoon continued to move northwest and hit Guangxi (GX) province. Although its intensity was weakened gradually along its path, the heavy rains and strong storms brought by Typhoon Mangkhut still affected four other provinces including Fujian (FJ), Hainan (HI), Guizhou (GZ), and Yunnan (YN), causing direct economic losses of 5.2 billion yuan. The geographical position of the main affected provinces in Typhoon Mangkhut and the typhoon path are shown in Fig. 13. The darker gray represents more severe damage to transport services. According to its wind speed and destructive power, Typhoon Mangkhut is typically T3-grade in GD province.

The typhoon event had severe consequences on HRN and CAN in affected provinces, and they took 37 h and 12 h to fully recover, respectively. Values of resilience metrics in Typhoon Mangkhut are shown in Table 3. Both HRN and CAN are severely affected in this typhoon: nearly half of both flights and trains were delayed or canceled. The performance losses (V) of CAN is only slightly larger and its performance decreases slightly faster. The recovery speed of CAN is much more dominant as its recovery rapidity (E) is much larger than HRN. Due to this, CAN is more resilient than HRN. This is consistent with analyses in T3-grade typhoon scenarios. The resilience of the combined system is 0.8213, while that of complementary system is 0.8230. This difference shows the positive influence of complementary effects. As discussed in Section 4.3, this difference is not large in T3-grade typhoons indeed. But considering the large number of all passengers and the total transportation capacity in the whole network, this difference is still a great number of trips.

According to the sensitivity analysis in Section 4.4, we have known that increasing the spare capacity of HRN is effective to increase system resilience for T1- and T2-grade typhoon scenarios, and that increasing recovery rapidity of HRN is effective for T2- and T3-grade typhoon scenarios. Notice that the influence of Typhoon Mangkhut in each affected province is different, which is shown in Fig. 13. Therefore, we consider a combined measure to improve the system performance in this case: The spare capacities of HRN in provinces suffering T1- and T2-grade influences (i.e. provinces YN, GZ, FJ, GX and HI) are increased and the recovery rapidities of HRN in provinces suffering T2- and T3-grade influences (i.e. provinces GX, HI and GD) are increased. The change in percentage of system resilience under enhancement measures are shown in Fig. 14.

Table 3
Resilience metrics of transport networks under Typhoon Mangkhut.

Network	R'	Resilience factors ($\times 10^4$)			
		V	D	E	A
HRN	0.7994	−350	−10.2	10.9	350
CAN	0.8789	−140	−4.09	35.0	140

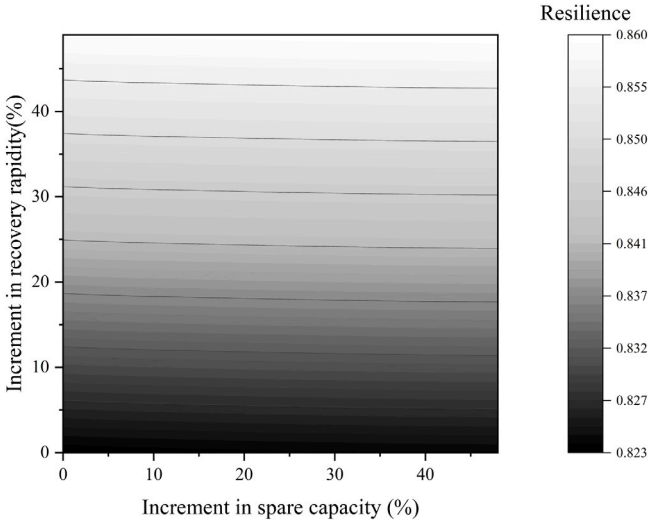

Fig. 14. Contour plot of resilience with respect to increments in spare capacity and recovery rapidity.

It is apparently that increasing the recovery rapidity of HRN is much more effective than increasing the spare capacity of HRN in this case. This is because in T3-grade typhoon scenarios, reducing the recovery time can improve the performance of HRN greatly. Therefore, for regions prone to typhoon events whose magnitude is similar to Typhoon Mangkhut, decision-makers should consider enhancing the pre- and post-disaster response for HRN to improve its recovery rapidity, which is promising to achieve a better performance level of the whole transportation system.

6. Concluding remarks

In this paper, we introduce a group of metrics to assess the resilience of transportation systems under natural disasters. These metrics are useful to show different characteristics of transportation networks. Based on these metrics, a time-dependent and flow-based metric for system resilience is proposed, which can reflect the change of system performance at each phase. Note that networks with the same value of resilience may have very different values in the specific metrics. This is the basis for cooperation between HRN and CAN aiming to enhance the resilience of the two networks. Then we investigate the complementary effects between HRN and CAN on the system resilience in typhoon scenarios. Typhoon scenarios with different damage strengths are simulated by using a Spatially Localized Failure model and the Monte Carlo method.

The proposed framework has been applied to Chinese HRN and CAN in simulated typhoon scenarios and also the real case of Typhoon Mangkhut. The results show that HRN and CAN have different resilience characteristics. In T1-grade typhoon scenarios, the resilience of HRN keeps almost unchanged, but that of CAN decreases a lot. This shows that HRN has a greater resistance capacity than CAN in weak typhoons. It also explains why the number of passengers in a complementary system of the two networks increases a lot. In T2-grade typhoon scenarios, both networks suffer great decreases in resilience. The increased number of passengers also decreases. In T3-grade typhoon scenarios, both networks are vulnerable and thus keep low resilience levels, but CAN is slightly better due to its promising nature in recovery rapidity. The increased number of passengers decreases to a lower level but is not close to zero due to the support of CAN in the complementary effects. By taking advantage of the complementary effects between the two networks, cooperation between HRN and CAN can enhance the system resilience. We have studied the effects of two resilience enhancement measures, i.e., increasing spare capacity and increasing recovery rapidity. These measures can be accomplished by operations such as spared transportation equipment and prepositioned rescue personnel and equipment, which are common in practice. We find that in T1-grade typhoons, increasing the spare capacity of HRN is effective in enhancing system resilience in a complementary system. In T2-grade typhoon scenarios, increasing the spare capacity and recovery rapidity of HRN are more effective. In T3-grade typhoon scenarios, increasing the recovery rapidity of HRN significantly enhances system resilience. The recovery rapidity of HRN plays an important role in strong typhoon scenarios. This is because both HRN and CAN are badly affected. As HRN has a much larger transport capacity in China, increasing the recovery rapidity of HRN deserves much more effort.

We examine the influence of transport capacity in system resilience by manipulating the transport capacity ratio of HRN and CAN in our model. The results confirm that if the transport capacity of CAN is increased, the system resilience decreases in weak typhoon scenarios but increases in strong typhoon scenarios.

All our findings support the argument that proper cooperation between transportation system with different resilience characteristics improves complementary resilience. We provide metrics corresponding to the four phases of a disruption to address the resilience characteristics of a transportation system. Numerical results based on simulations have verified the effectiveness of resilience enhancement strategies.

There are some limitations of this research that deserve further explorations. The first one is the simplification of transfers in transportation systems. The transfer of passengers only depends on the available capacity of alternative trains/flights, ignoring the transfer willingness of passengers and timetables of trains/flights. As the consequence, travel demands are considered to be within-day and thus the day-to-day spillover effects of delayed trips are ignored in our model. To resolve this issue, not only the traveler's behaviors based on utility maximization have to be modeled, the transfer capacity of transition stations and the timetable or schedule of trains/flights also need to be taken into account. This work requires an evolved framework for transportation systems, which is among our future tasks. The second limitation relates to the practical implementation. Due to the available data and the disaster emergence operations in practice, we considered impact of typhoons and resilience enhancement at a province level. With improvement of observations and data collections in future, fine management at a more detailed level should be the trend.

Data availability

Data will be made available on request.

Acknowledgments

This work was partially supported by the National Natural Science Foundation of China (Grant 72171191) and the Natural Science Basic Research Program of Shaanxi, China (Grant 2021JM-026).

References

Adams, T.M., Bekkem, K.R., Toledo-Durán, E.J., 2012. Freight resilience measures. J. Transp. Eng. 138 (11), 1403–1409.
Adjetey-Bahun, K., Birregah, B., Châtelet, E., Planchet, J.-L., 2016. A model to quantify the resilience of mass railway transportation systems. Reliab. Eng. Syst. Saf. 153, 1–14.
Aghababaei, M., Costello, S.B., Ranjitkar, P., 2020. Transportation impact assessment following a potential alpine fault earthquake in New Zealand. Transp. Res. Part D 87, 102511.
Argyroudis, S.A., Mitoulis, S.A., Hofer, L., Zanini, M.A., Tubaldi, E., Frangopol, D.M., 2020. Resilience assessment framework for critical infrastructure in a multi-hazard environment: Case study on transport assets. Sci. Total Environ. 714, 136854.
Avenali, A., Bracaglia, V., D'Alfonso, T., Reverberi, P., 2018. Strategic formation and welfare effects of airline-high speed rail agreements. Transp. Res. B 117, 393–411.
Baggag, A., Abbar, S., Zanouda, T., Srivastava, J., 2018. Resilience analytics: coverage and robustness in multi-modal transportation networks. EPJ Data Sci. 7, 1–21.
Barker, K., Ramirez-Marquez, J.E., Rocco, C.M., 2013. Resilience-based network component importance measures. Reliab. Eng. Syst. Saf. 117, 89–97.
Baroud, H., Barker, K., Ramirez-Marquez, J.E., et al., 2014. Importance measures for inland waterway network resilience. Transp. Res.Part E 62, 55–67.
Berdica, K., 2002. An introduction to road vulnerability: what has been done, is done and should be done. Transp. Policy 9 (2), 117–127.
Chen, L., Miller-Hooks, E., 2012. Resilience: an indicator of recovery capability in intermodal freight transport. Transp. Sci. 46 (1), 109–123.
Chen, Z., Wang, Y., 2019. Impacts of severe weather events on high-speed rail and aviation delays. Transp. Res. Part D 69, 168–183.
D'Alfonso, T., Jiang, C., Bracaglia, V., 2015. Would competition between air transport and high-speed rail benefit environment and social welfare? Transp. Res. B 74, 118–137.
D'Lima, M., Medda, F., 2015. A new measure of resilience: An application to the London underground. Transp. Res. Part A 81, 35–46.
Fang, C., Dong, P., Fang, Y.-P., Zio, E., 2020. Vulnerability analysis of critical infrastructure under disruptions: An application to China railway high-speed. Proc. Inst. Mech. Eng. Part O 234 (2), 235–245.
Fang, Y.-P., Fang, C., Zio, E., Xie, M., 2019. Resilient critical infrastructure planning under disruptions considering recovery scheduling. IEEE Trans. Eng. Manage..
Fang, Y.-P., Pedroni, N., Zio, E., 2016. Resilience-based component importance measures for critical infrastructure network systems. IEEE Trans. Reliab. 65 (2), 502–512.
Fang, Y., Zio, E., 2019. Game-theoretic decision making for the resilience of interdependent infrastructures exposed to disruptions. In: Critical Infrastructure Security and Resilience. Springer, pp. 97–114.
Faturechi, R., Miller-Hooks, E., 2014. A mathematical framework for quantifying and optimizing protective actions for civil infrastructure systems. Comput.-Aided Civ. Infrastruct. Eng. 29 (8), 572–589.
Henry, D., Ramirez-Marquez, J.E., 2012. Generic metrics and quantitative approaches for system resilience as a function of time. Reliab. Eng. Syst. Saf. 99, 114–122.
Holling, C.S., 1973. Resilience and stability of ecological systems. Annu. Rev. Ecol. Syst. 4 (1), 1–23.
Hong, L., Ouyang, M., Peeta, S., He, X., Yan, Y., 2015. Vulnerability assessment and mitigation for the Chinese railway system under floods. Reliab. Eng. Syst. Saf. 137, 58–68.
Van der Hurk, E., Koutsopoulos, H.N., Wilson, N., Kroon, L.G., Maróti, G., 2016. Shuttle planning for link closures in urban public transport networks. Transp. Sci. 50 (3), 947–965.
Ip, W.H., Wang, D., 2011. Resilience and friability of transportation networks: evaluation, analysis and optimization. IEEE Syst. J. 5 (2), 189–198.
Janić, M., 2015. Reprint of ''modelling the resilience, friability and costs of an air transport network affected by a large-scale disruptive event''. Transp. Res. Part A 81, 77–92.
Jin, J.G., Tang, L.C., Sun, L., Lee, D.-H., 2014. Enhancing metro network resilience via localized integration with bus services. Transp. Res. Part E 63, 17–30.
Jin, J.G., Teo, K.M., Odoni, A.R., 2016. Optimizing bus bridging services in response to disruptions of urban transit rail networks. Transp. Sci. 50 (3), 790–804.

Li, T., Rong, L., 2019. Resilience of air transport network with the complementary effects of high-speed rail network. In: 2019 IEEE 19th International Conference on Software Quality, Reliability and Security Companion (QRS-C). IEEE, pp. 348–353.
Liang, J., Wu, J., Qu, Y., Yin, H., Qu, X., Gao, Z., 2019. Robust bus bridging service design under rail transit system disruptions. Transp. Res. Part E 132, 97–116.
Luo, C., Xu, L., 2021. Railway disruption management: Designing bus bridging services under uncertainty. Comput. Oper. Res. 131, 105284.
Nan, C., Sansavini, G., 2017. A quantitative method for assessing resilience of interdependent infrastructures. Reliab. Eng. Syst. Saf. 157, 35–53.
Ouyang, M., Pan, Z., Hong, L., He, Y., 2015. Vulnerability analysis of complementary transportation systems with applications to railway and airline systems in China. Reliab. Eng. Syst. Saf. 142, 248–257.
Ouyang, M., Tian, H., Wang, Z., Hong, L., Mao, Z., 2019. Critical infrastructure vulnerability to spatially localized failures with applications to Chinese railway system. Risk Anal. 39 (1), 180–194.
Panteli, M., Mancarella, P., 2015. Modeling and evaluating the resilience of critical electrical power infrastructure to extreme weather events. IEEE Syst. J. 11 (3), 1733–1742.
Reichardt, U., Ulfarsson, G.F., Pétursdóttir, G., 2018. Volcanic ash and aviation: recommendations to improve preparedness for extreme events. Transp. Res. Part A 113, 101–113.
Stamos, I., Mitsakis, E., Salanova, J.M., Aifadopoulou, G., 2015. Impact assessment of extreme weather events on transport networks: A data-driven approach. Transp. Res. Part D 34, 168–178.
Takagi, H., Yi, X., Fan, J., 2021. Public perception of typhoon signals and response in macau: did disaster response improve between the 2017 Hato and 2018 Mangkhut typhoons? Georisk: Assess. Manage. Risk Eng. Syst. Geohazards 15 (1), 76–82.
Verschuur, J., Koks, E., Hall, J., 2020. Port disruptions due to natural disasters: Insights into port and logistics resilience. Transp. Res. Part D 85, 102393.
Wan, C., Yang, Z., Zhang, D., Yan, X., Fan, S., 2018. Resilience in transportation systems: a systematic review and future directions. Transp. Rev. 38 (4), 479–498.
Wang, Y., Guo, J., Currie, G., Ceder, A., Dong, W., Pender, B., 2014. Bus bridging disruption in rail services with frustrated and impatient passengers. IEEE Trans. Intell. Transp. Syst. 15 (5).
Zeng, G., Sun, Z., Liu, S., Chen, X., Li, D., Wu, J., Gao, Z., 2021. Percolation-based health management of complex traffic systems. Front. Eng. Manage. 8, 531–544.
Zhang, S., Lo, H.K., 2018. Metro disruption management: Optimal initiation time of substitute bus services under uncertain system recovery time. Transp. Res. C 97, 409–427.
Zhang, P., Peeta, S., 2011. A generalized modeling framework to analyze interdependencies among infrastructure systems. Transp. Res. B 45 (3), 553–579.
Zhou, L., Chen, Z., 2020. Measuring the performance of airport resilience to severe weather events. Transp. Res. Part D: Transp. Environ. 83, 102362.